First-principles study of surface properties of $LiFePO_4$: Surface energy, structure, Wulff shape, and surface redox potential

L. Wang, F. Zhou, Y. S. Meng, and G. Ceder*

Department of Materials Science and Engineering, Massachusetts Institute of Technology, Cambridge, Massachusetts 02139, USA

(Received 16 March 2007; revised manuscript received 4 August 2007; published 26 October 2007)

Using first-principles calculations within the generalized gradient approximation (GGA)+U framework, we investigate several surface properties of olivine structure $LiFePO_4$. Calculated surface energies and surface redox potentials are found to be very anisotropic. Low-energy surfaces are in the [1 0 0], [0 1 0], [0 1 1], [1 0 1], and [2 0 1] orientations of the orthorhombic structure. We find that the coordination loss of Fe atoms on the surface is energetically more unfavorable than for Li, and generally a low-energy surface has fewer Fe-O bonds affected by the surface cut. Conversely, undercoordinated Li on the surface are somehow beneficial to reduce the energy of a surface except for the twofold coordinated Li. With the calculated surface energies, we provide the thermodynamic equilibrium shape of the $LiFePO_4$ crystal through a Wulff construction. The two low-energy surfaces (0 1 0) and (2 0 1) dominate in the Wulff shape and make up almost 85% of the surface area. Similar calculations for $FePO_4$ indicate a very low energy for the (0 1 0) surface of $FePO_4$. This result suggests that surface chemistry can induce a change in the aspect ratio of the Wulff shape. Surface redox potentials for the extraction and insertion of Li from various surfaces are also investigated in this work. The Li redox potential for the (0 1 0) surface is calculated to be 2.95 V, which is significantly lower than the bulk value of 3.55 V. For several other surfaces the Li extraction potential is above the bulk potential. We also develop a simple model that can be used to predict surface energies based on the change in the coordination of Fe and Li.

DOI: 10.1103/PhysRevB.76.165435 PACS number(s): 68.35.Md, 68.43.Bc, 68.47.Gh

I. INTRODUCTION

$LiFePO_4$ has appeared as a promising cathode material for high-power rechargeable lithium-ion batteries, but much of its unusual phase behavior and transport properties remain to be understood. The orthorhombic olivine structure of $LiFePO_4$ has a space group of *Pnma* and is rather anisotropic in many of its properties. Maxisch *et al.*[1] calculated the elastic moduli for $LiFePO_4$ and the delithiated $FePO_4$ form of it, and found significant variations along the three orthorhombic directions. Due to the nature of the olivine crystal structure, the variation in the transport properties is even more significant. The *ab initio* study of Morgan *et al.* indicated that while Li^+ mobility is high in the tunnels along the [0 1 0] direction, Li^+ hopping between tunnels is very unlikely.[2] Similar conclusions were reached by Islam *et al.* using potential models.[3] Recently, transport measurements on single crystalline $LiFePO_4$ have also become available.[4] Early in the development of $LiFePO_4$, it was thought that the material's charge/discharge rate was limited by electronic transport, leading to the development of doping[5] and carbon coating techniques[6–8] to improve the apparently low electronic conductivity of the material. It has also been suggested that the transport limitations can be overcome by using small particles.[6,9] Recently, fairly good electrochemical performance has been achieved without the use of carbon coating by reducing particle size to about 140 nm.[10]

However, given the anisotropic nature of the material, control of particle shape may be as important as average size control. This has stimulated research in new synthesis routes for $LiFePO_4$. Starting with the pioneering work of Whittingham's group[11,12] and more recently work by other research groups,[13–16] well crystallized particles of $LiFePO_4$ can be formed via a hydrothermal approach. More interestingly, several studies reported platelet shape $LiFePO_4$ crystals in the hydrothermal synthesis.[11,17] Electron microscopy studies by Richardson *et al.*[18] showed that the large facet of the platelike crystals is the (0 1 0) surface. Given the one-dimensional Li diffusion path along the [0 1 0] direction, Richardson *et al.*[18] further suggested that the use of thin, unagglomerated particles with large (010) surface area would increase the active area and decrease the diffusion distances for Li ions. For a crystal in its thermodynamic equilibrium shape, the relative area of each facet on a particle depends on its surface energy. In the case of plate-type $LiFePO_4$, a preference of the (0 1 0) facet on the crystal implies that the (0 1 0) surface is thermodynamically favored over other facets. The objective of this paper is to investigate the surface energy, structure, and redox potential of important facets.

First-principles investigations of surfaces and the calculations of surface energies are well-established for metal oxides.[19–23] Our studies start from stoichiometric surfaces of $LiFePO_4$. Once the surface energies are calculated, the thermodynamic equilibrium shape of a crystal can be determined through the Wulff construction (explained in the next section).[24] For the thermodynamically stable facets in the Wulff shape, we further calculate the surface redox potentials as the average energy (per formula unit of Li) to extract (insert) Li from (into) the outermost layer of a given surface. We find somewhat surprisingly that on some surfaces the redox potential is above the bulk value, while on others it is below, indicating that Li extraction/insertion may occur in a nontrivial manner, inconsistent with a core-shell model of delithiation.

II. METHODOLOGY

All total energies in this work are calculated using the generalized gradient approximation (GGA) to the density

functional theory (DFT). The projected augmented wave[25] (PAW) method is used, as implemented in the Vienna *ab initio* simulation package (VASP).[26] An energy cutoff of 400 eV and appropriate k-point meshes are chosen to ensure that the total energies are converged within 3 meV per formula unit of $LiFePO_4$. Electron correlation within the d states significantly affects the electronic structure and energetic properties of transition metal oxides.[27–31] The GGA $+U$ approach[32,33] is used to accurately calculate the surface redox potentials and to guarantee that the excess holes or electrons are properly localized. For details about the implementation of the GGA$+U$ approach within a PAW framework, the readers can refer to the work of Bengone *et al.*[34] Quantitative results in the GGA$+U$ method are known to depend on the value of U and the choice of the expression for the double-counting term. The value of U depends on the valence state of the transition-metal ion and crystal environment.[28,35] In this work, we choose a J value of 1 eV and a U value of 5.3 eV, which is the average of the self-consistently calculated U values for Fe^{2+} (U=4.7 eV in $LiFePO_4$) and Fe^{3+} (U=5.9 eV for $FePO_4$).[28] We found the values of the surface energies to vary less than 3% as the U value decreases from 5.3 to 4.7 eV. The appropriateness of different double counting schemes has been discussed in Ref. 36. While for moderately correlated system it is still not clear how to capture best the double counting energy, there is little ambiguity as to the appropriateness of GGA$+U$ for insulators with strong localization,[36] as is the case in Li_xFePO_4. We employ the "fully localized" double counting scheme as presented by Liechtenstein *et al.*[37] Previous GGA$+U$ calculations on $LiFePO_4$ indicate that this U parameter and double counting scheme provide for good agreement with experiment. The detailed discussions can be found in Refs. 27 and 28. A ferromagnetic high-spin Fe state is assumed. The bulk $LiFePO_4$ ($FePO_4$) is paramagnetic at room temperature[38] and the energetic effects of the magnetic ordering are small.[39]

The lattice parameters of the relaxed bulk $LiFePO_4$ structure are a=10.4363 Å, b=6.0491 Å, c=4.7546 Å, in good agreement with experiments.[38] Figure 1 shows the crystal structure of bulk $LiFePO_4$ after relaxation. The initial unrelaxed surface structures are carved out of the fully relaxed bulk crystal. In principle, a surface with a given Miller index can terminate anywhere along the direction of surface normal. However, in this study we only consider stoichiometric surfaces for the investigation of surface energies. Under this assumption, the candidate planes for surface terminations are limited. For example, to create a stoichiometric (1 0 0) surface, the possible termination planes are $(0.5,y,z)$ and $(0.25,y,z)$ (expressed in fractional coordinates for the unit cell setting in Fig. 1). Other terminations in this orientation will create either a nonstoichiometric surface, or a surface that is equivalent to any of the two mentioned above. For atoms that lie on the cutting plane, the following principles have been additionally adopted.

(1) The PO_4 tetrahedron is always preserved if the surface termination cuts through it, and a corrugated surface may be created. As shown in Fig. 1(a), the tentative termination plane $(0.5,y,z)$ for the (1 0 0) surface would cut through the highly covalent P-O bonds and create a surface with the undercoordinated P being exposed on top of the surface. Our calculations suggest that such a surface has a very high surface energy. Thus, in practice a neighboring Fe atom is left undercoordinated in order to keep the PO_4 tetrahedron intact.

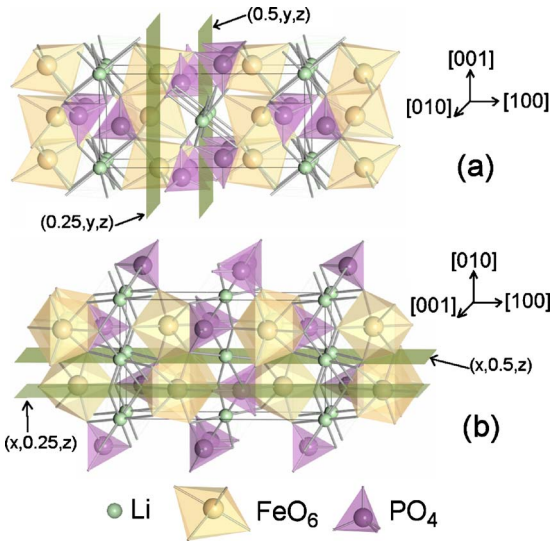

FIG. 1. (Color online) Relaxed crystal structure of bulk $LiFePO_4$ and possible planes for surface terminations in two orientations. Panel (a) shows for the (1 0 0) surface the two possible cuts containing points $(0.25,y,z)$ and $(0.5,y,z)$, respectively. Panel (b) shows for the (0 1 0) surface the two termination planes $(x,0.25,z)$ and $(x,0.5,z)$, respectively.

(2) For an ionic or partially ionic crystal, it is known that a charged surface with a perpendicular dipole moment will induce a polarizing electric field throughout the crystal, resulting in a very large surface energy.[40] Hence, all the surfaces studied in this work are "type II" or "type III" surfaces according to the classification by Tasker,[40] with a vanishing dipole in the direction of the surface normal.

(3) The ion coordination loss at the surface should be minimized. This rule is practically useful as various stoichiometric surface configurations can be created at the termination plane. The stable surfaces are expected to have low ion coordination loss.

The candidate planes for surface terminations can also be narrowed down by applying the third rule described above. For example, for the (0 1 0) surface, the cut at plane $(x,0.5,z)$ in Fig. 1(b) would have two Fe-O bonds and three Li-O bonds cut per $a\times c$ unit surface area. However, if the surface terminates at plane $(x,0.25,z)$ in Fig. 1(b), the coordination number loss would further increase to five Fe-O bonds and three Li-O bonds on the same surface area. Thus, a surface terminating at plane $(x,0.5,z)$ is expected to give a lower surface energy than the one at plane $(x,0.25,z)$. For several orientations it is not possible to predetermine which of the different surface configurations will be lower in energy. For example, surface (1 0 0) has one Fe-O bond and three Li-O bonds (per surface area of $b\times c$) broken if cut at plane $(0.5,y,z)$ in Fig. 1(a). Conversely, it would have three broken Fe-O bonds and no broken Li-O bond on the same surface area if cleaving at plane $(0.25,y,z)$ in Fig. 1(a). Therefore, multiple termination possibilities are calculated for those directions where possible.

TABLE I. Surface energies of $LiFePO_4$ in seven low-index directions together with values for (2 0 1) and (3 0 1) surfaces.

Orientation	(100)	(010)	(001)	(101)	(011)	(110)	(111)	(201)	(301)
$\gamma(J/m^2)$	0.66	0.64	0.97	0.62	0.76	1.30	0.85	0.52	0.62

For each possible surface termination, the surface is then simulated using the slab technique, in which a set of infinite layers separated by vacuum layers are repeated periodically along the surface normal. We have chosen our slabs such that the two sides of it are symmetrically equivalent and can be mapped into each other by an inversion, mirror or glide type of symmetry operation in the middle of the slab. This is possible for $LiFePO_4$ due to the particular space group of $P\,2_1/n\,2_1/m\,2_1/a$ (the full convention). In the olivine crystal structure, positions with inversion symmetry are 4*a* sites [(0, 0, 0), (0.5, 0, 0.5), (0, 0.5, 0), (0.5, 0.5, 0.5)] and 4*b* sites [(0, 0, 0.5), (0.5, 0, 0), (0, 0.5, 0.5), (0.5, 0.5, 0)]. Moreover, there are mirror and glide symmetries perpendicular to the three principal axes of the orthorhombic unit cell. In Ref. 20 and Refs. 41–49, where the slab model is employed to investigate surface properties with *ab initio* methods, readers can find more examples of using symmetry of underlying crystal structure to ensure that the stoichometric surfaces on each side of the slab give the same structure configuration and energy.

In our study, lattice parameters of the supercell (including slab and vacuum) are fixed and only atoms near the surface are allowed to relax until forces are smaller than 0.03 eV/Å. The inner part of the slab is frozen at bulk positions to simulate the bulk of this material. The thicknesses of vacuum, slab and free relaxation layer are all varied to obtain a surface energy in the given direction converged to within 5% of the calculated value.

The equilibrium shape of a crystal is related to the surface energies through the Wulff construction.[24] A polar plot of the surface energy can be constructed by drawing along each crystallographic orientation *n* a vector whose norm equals the surface energy in this direction. A plane perpendicular to each vector is then drawn passing through the endpoint of the vector. The inner envelope of all these planes forms the Wulff construction and only planes that are part of the Wulff shape are thermodynamically stable.

III. RESULTS

A. Surface energies

Surface energies are calculated by taking the difference between the energy of our slab and the same amount of $(Li)FePO_4$ formula units in the bulk, divided by the surface area of the slab (including both sides of the slab):

$$\gamma = \frac{E_s - nE_b}{2S}. \quad (1)$$

Here, E_b is the total energy per formula unit of bulk $LiFePO_4$. E_s is the total energy of the given supercell containing *n* formula units of $LiFePO_4$. *S* is the base area of the supercell. In this section, only the surface energies for the most stable configurations are reported. Surface energies for the high energy cuts are reported in the next section.

To test convergence, we examined how the calculated surface energies vary with respect to the thickness of the vacuum layer. A vacuum layer of 10 Å is found to be enough to remove any spurious interaction between the periodically repeated slabs in the direction of surface normal. We also investigated how the calculated surface energies vary with respect to the thickness of the slab and relaxation layer. Results from these convergence tests for each surface are provided in the next section together with a discussion on the surface relaxations.

The calculated surface energies for seven low-index surfaces are summarized in Table I. Among the seven low-index orientations, surface (0 1 0), (1 0 0), and (1 0 1) have the lowest energies. While it is not practical to study all high-index surfaces, several surfaces that potentially have low energies are studied in this work. Based on the calculated surface energies in low-index orientations and noting that surface (1 0 1) has the lowest energy among the nonprincipal directions, we also investigated the (2 0 1) and (3 0 1) surfaces, which are indeed calculated to be low energy surfaces. Although one can argue that other high-index surfaces may influence the thermodynamic stability of the nine surfaces studied here, as we discuss later, the crystal morphology is not significantly modified by including more high-index surfaces.

B. Surface relaxations

To investigate how the surface energy relates to the surface structure, we will show the relaxed surface structures in this section and provide the displacements of undercoordinated ions on the surfaces. Energetics for the high-energy terminations in each orientation are also provided.

1. The (1 0 0) surface

We find that the low-energy cut in this direction terminates at point (0, 0, 0) [a plane symmetrically equivalent to plane $(0.5, y, z)$ in Fig. 1(a)]. A slab of 11.3 Å with a relaxation layer of 3.9 Å is sufficient to get a converged surface energy. The surface termination cuts through the LiO_6 octahedra and one vertex of the PO_4 tetrahedra. As mentioned in the methodology section, we keep the PO_4 tetrahedra intact because of the strong covalent P-O bonds, consequently, the nearby FeO_6 octahedra are cut instead. In the original unrelaxed structure, the $Li_{(1)}$ on the surface are threefold coordinated by oxygen, and fivefold coordinated $Fe_{(1)}$ are buried farther below the surface. The relaxed structure is shown in Fig. 2 and the detailed relaxations are provided in Table II.

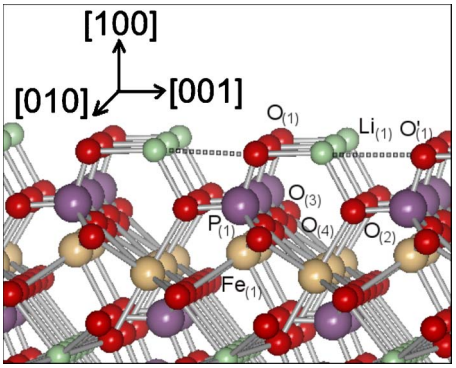

FIG. 2. (Color online) The relaxed surface structure of (1 0 0) surface. Color setting for the Li, Fe, and P atoms is the same as in Fig. 1. Oxygen atoms are shown as red. The undercoordinated ions are labeled. The dotted lines mean that the two atoms $Li_{(1)}$ and $O'_{(1)}$, are probably not bonded because of the large distance between them.

Note that while the displacements given here are absolute values, they can also be considered relative to the bulk, as the unit cell does not move as a whole because the atoms 3 Å below the surface undergo only minor displacements. The $Li_{(1)}$ atom relaxes most. It is originally coordinated with $O_{(1)}$, $O_{(2)}$, and $O_{(3)}$ (see Fig. 2) but relaxes toward the twofold "bridging" $O'_{(1)}$ atom in the neighboring row of O atoms, and loses its bonding with $O_{(3)}$. The distance between $Li_{(1)}$ and $O'_{(1)}$ is about 2.9 Å, which is much larger than the average bond length of 1.85 Å for $Li_{(1)}$-$O_{(1)}$ and $Li_{(1)}$-$O_{(2)}$ bonds on the surface. Therefore, we consider the $Li_{(1)}$ to be twofold coordinated after the relaxations. The fivefold $Fe_{(1)}$ lies well beneath the surface and its relaxation is negligibly small. We also studied another possible surface cut in the (1 0 0) direction which terminates at point (0.25, 0, 0) [see plane $(0.25, y, z)$ in Fig. 1(a)]. This surface cut leaves the threefold coordinated Fe atoms directly exposed on the surface, and is

TABLE II. Relaxations (displacements Δu, Δv, and Δw are in Å) of undercoordinated Li, Fe, and O atoms on the nine surfaces. Only displacements larger than 0.1 Å are provided. The directions of the u, v, and w axes are consistent with the axes shown in Figs. 2–10, e.g., the u, v, and w axes for the (1 0 0) surface lie along the [0 1 0], [0 0 1], [1 0 0] directions, respectively, as shown in Fig. 2. Atom labels also refer to Figs. 2–10.

Surface	Label	Coord.	Δu	Δv	Δw	Surface	Label	Coord.	Δu	Δv	Δw	Surface	Label	Coord.	Δu	Δv	Δw
(100)	$Li_{(1)}$	2	1.47	0.17	0.61	(011)	$Li_{(1)}$	3	−0.37	−1.57	−0.12	(101)	$Li_{(1)}$	3	−0.17	0.29	−0.32
	$Fe_{(1)}$	5	−0.14	0.08	−0.08		$Li_{(2)}$	4	−0.10	0.51	0.02		$Li_{(2)}$	3	−0.10	0.21	−0.42
	$P_{(1)}$	4	−0.14	−0.13	0.09		$Li_{(3)}$	5	−0.05	−0.34	−0.10		$Fe_{(2)}$	4	−0.02	0.00	−0.32
	$O_{(1)}$	2	−0.03	−0.29	0.12		$Fe_{(1)}$	4	−0.02	−0.21	−0.46		$O_{(2)}$	2	0.04	0.16	−0.04
	$O_{(2)}$	3	−0.08	−0.13	0.01		$Fe_{(2)}$	4	−0.05	0.31	−0.47		$O_{(4)}$	3	−0.04	0.14	−0.06
	$O_{(3)}$	3	−0.21	−0.19	0.16		$O_{(1)}$	1	−0.08	−0.25	0.00		$O_{(6)}$	3	0.04	−0.11	−0.04
	$O_{(4)}$	3	−0.20	−0.13	−0.05		$O_{(2)}$	2	−0.14	0.09	0.01	(110)	$Li_{(1)}$	4	0.16	2.95	−0.19
(010)	$Li_{(1)}$	3	−0.07	−0.35	−0.09		$O_{(4)}$	3	0.03	0.14	−0.05		$Fe_{(1)}$	3	−0.50	−0.83	−0.48
	$Fe_{(1)}$	5	0.23	0.06	−0.09		$O_{(5)}$	3	0.02	−0.14	−0.07		$Fe_{(2)}$	5	0.26	0.32	−0.03
	$Fe_{(2)}$	5	−0.19	−0.12	−0.08	(301)	$Li_{(1)}$	4	−0.11	−0.05	0.00		$P_{(2)}$	4	0.15	−0.07	0.07
	$P_{(1)}$	4	0.18	−0.15	0.07		$Li_{(2)}$	4	0.11	−0.05	0.00		$O_{(1)}$	2	−0.05	0.38	−0.04
	$O_{(1)}$	3	0.04	−0.19	−0.07		$Li_{(3)}$	4(5)	−0.19	−0.21	0.03		$O_{(2)}$	3	0.06	−0.02	−0.16
	$O_{(2)}$	2	0.28	−0.40	−0.12		$Li_{(4)}$	4(5)	0.19	−0.20	0.02		$O_{(3)}$	3	0.05	−0.04	0.15
	$O_{(3)}$	3	0.32	−0.11	0.29		$Fe_{(1)}$	5	0.00	−0.17	−0.07		$O_{(5)}$	3	0.17	−0.02	0.10
	$O_{(4)}$	3	0.17	−0.19	−0.09		$Fe_{(2)}$	4	0.00	−0.14	−0.12	(111)	$Li_{(1)}$	3	−0.016	0.49	−0.49
(001)	$Li_{(1)}$	3	0.07	0.02	−0.37		$Fe_{(3)}$	5	−0.01	0.25	0.10		$Li_{(2)}$	4	−0.10	0.00	−0.34
	$Li_{(2)}$	5	−0.17	0.02	−0.14		$Fe_{(4)}$	5	0.00	0.06	−0.11		$Li_{(3)}$	5	−0.22	−0.15	−0.36
	$Li_{(3)}$	5	0.24	−0.04	−0.11		$P_{(1)}$	4	−0.01	−0.18	0.09		$Fe_{(1)}$	3	−0.02	0.01	−0.45
	$Fe_{(1)}$	3	0.07	−0.03	−0.49		$P_{(3)}$	4	0.00	0.16	0.04		$Fe_{(2)}$	4	−0.02	0.10	−0.73
	$Fe_{(2)}$	5	0.00	−0.13	0.04		$O_{(1)}$	1	0.00	−0.41	−0.06		$P_{(2)}$	4	−0.18	−0.15	−0.12
	$P_{(1)}$	4	0.05	−0.12	0.07		$O_{(2)}$	3	0.01	−0.16	−0.02		$O_{(1)}$	2	0.21	−0.10	−0.17
	$O_{(2)}$	3	0.07	0.00	−0.13		$O_{(3)}$	3	−0.03	−0.14	−0.02		$O_{(2)}$	3	−0.16	0.24	−0.14
(201)	$Li_{(1)}$	3	0.14	−0.46	−0.14		$O_{(7)}$	2	0.00	0.15	−0.08		$O_{(3)}$	2	−0.39	−0.38	−0.22
	$Li_{(2)}$	5(4)	−0.17	−0.15	−0.04		$O_{(8)}$	3	0.00	0.24	−0.10		$O_{(4)}$	2	−0.04	0.22	−0.31
	$Li_{(3)}$	5(4)	0.15	−0.13	−0.05		$O_{(9)}$	3(4)	0.02	0.15	−0.02		$O_{(5)}$	3	0.05	−0.10	−0.21
	$Fe_{(1)}$	4	0.01	−0.18	−0.21		$O_{(10)}$	3(4)	−0.02	0.15	−0.02		$O_{(6)}$	3	−0.17	0.01	−0.33
	$Fe_{(2)}$	5	−0.02	−0.03	−0.15								$O_{(7)}$	3	−0.10	0.08	−0.16
	$O_{(3)}$	2	−0.04	−0.15	0.09								$O_{(8)}$	3	0.00	−0.04	−0.25
	$O_{(4)}$	3	0.03	−0.20	−0.01												

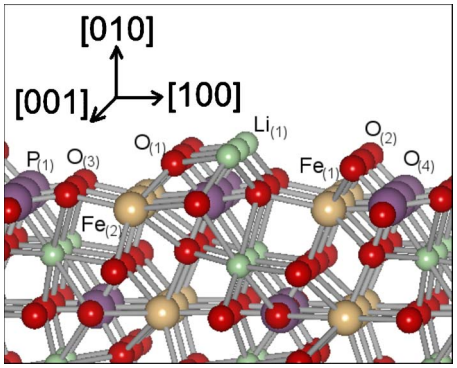

FIG. 3. (Color online) The relaxed surface structure of (0 1 0) surface.

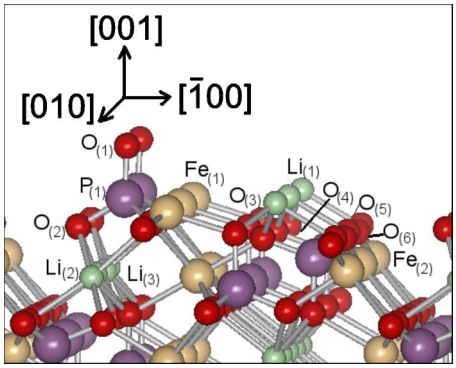

FIG. 4. (Color online) The relaxed surface structure of (0 0 1) surface.

calculated to have a somewhat higher surface energy of 0.73 J/m^2.

2. The (0 1 0) surface

The low-energy surface is found to terminate at point (0, 0, 0) [a plane equivalent to plane $(x,0.5,z)$ in Fig. 1(b)] with a surface energy calculated to be 0.64 J/m^2, compared with the much higher value of 1.21 J/m^2 if the surface is terminated at point (0, 0.25, 0) [see plane $(x,0.25,z)$ in Fig. 1(b)]. A slab of 12.1 Å with a relaxation layer of 3.3 Å is sufficient to get a converged surface energy for the low energy termination. The low energy termination in this direction cuts through the LiO_6 octahedra but only cuts the top of the FeO_6 octahedra, leaving threefold Li and fivefold Fe exposed on the surface. The relaxed structure of the low-energy termination is shown in Fig. 3 and the relaxations are provided in Table II. The threefold $Li_{(1)}$ is drawn toward one of three nearest-neighbor oxygen atom $O_{(1)}$ so that the length of the $Li_{(1)}$-$O_{(1)}$ bond decreases from 2.227 Å to 2.027 Å after the relaxations. The length of the bond between the fivefold $Fe_{(1)}$ and twofold $O_{(2)}$ drops from 2.274 Å to 2.076 Å because of the displacement of $O_{(2)}$ in the direction of [−1 0 0]. The distance between the fivefold $Fe_{(2)}$ and threefold $O_{(1)}$ is also reduced from 2.276 Å to 2.100 Å because of the displacement of $Fe_{(2)}$ in the direction of [0 0 1].

3. The (0 0 1) surface

In this direction, the low energy surface cut is found to terminate at point (0, 0, 0) and the surface energy is calculated to be 0.97 J/m^2. Another possible cut terminates at point (0, 0, 0.25) but results in a slightly higher surface energy of 1.02 J/m^2. For the low-energy termination, the relaxed structure is shown in Fig. 4 and the relaxations are given in Table II. A slab of 11.8 Å with a relaxation layer of 3.0 Å is used. The low energy termination cuts through the centers of FeO_6 octahedra and LiO_6 tetrahedra, so threefold $Fe_{(1)}$ and threefold $Li_{(1)}$ are exposed on the surface. The surface would also cut through the caps of the PO_4 tetrahedra, however, the $P_{(1)}$ tetrahedron is preserved by leaving the Fe and Li atoms in the layer immediately beneath undercoordinated. Therefore, the $Fe_{(2)}$, $Li_{(2)}$ and $Li_{(3)}$ are all fivefold coordinated. The $P_{(1)}$-$O_{(1)}$ bond sticks out in the direction of surface normal. Numbers for the (0 0 1) surface in Table II suggest that the dominating relaxations are the inward displacements of the $Li_{(1)}$ and $Fe_{(1)}$.

4. The (0 1 1) surface

The low-energy surface cut is found to terminate at point (0, 0, 0) with a calculated surface energy of 0.76 J/m^2. A slab of 7.5 Å with a relaxation layer of 2.5 Å is sufficient. Another possible cut terminates at point (0, 0.5, 0) but provides a much higher surface energy of 1.50 J/m^2. For the low-energy termination, the relaxed structure is shown in Fig. 5 and the relaxations are given in Table II. We can see that the surface cut runs through the centers of FeO_6 tetrahedra and LiO_6 tetrahedra leaving the $Fe_{(1)}$ and $Fe_{(2)}$ fourfold coordinated and the $Li_{(1)}$ threefold coordinated on the surface. The surface plane also cuts a cap of another LiO_6 tetrahedron which is not on the outermost surface, so $Li_{(2)}$ and $Li_{(3)}$ are left fivefold coordinated near the top surface. Numbers for the (0 1 1) surface in Table II suggest that the threefold $Li_{(1)}$ undergoes a substantial displacement in the [1 0 0] direction. The distances between $Li_{(1)}$ and the nearest-neighbor Fe atoms $Fe_{(1)}$ and $Fe_{(2)}$ are increased from 3.548 and 3.310 Å, to 4.431 and 5.214 Å, respectively. These in-

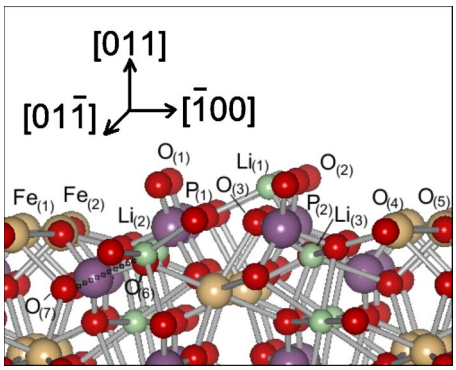

FIG. 5. (Color online) The relaxed surface structure of (0 1 1) surface.

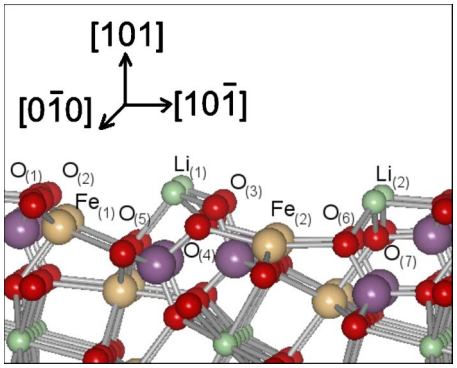

FIG. 6. (Color online) The relaxed surface structure of (1 0 1) surface.

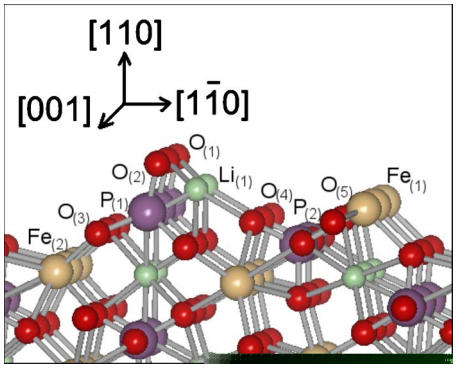

FIG. 7. (Color online) The relaxed surface structure of (1 1 0) surface.

creased separations between undercoordinated Li and Fe may be because the electrostatic repulsion between them is less effectively screened on the surface. There are substantial inward displacements for the threefold $Fe_{(1)}$ and $Fe_{(2)}$. For the fivefold $Li_{(2)}$, the displacement along the direction of [-1 0 0] increases the distance between $Li_{(2)}$ and $O_{(7)}$ from 2.228 to 2.617 Å. Therefore, we consider that the $Li_{(2)}$ is not bonded with $O_{(7)}$ any more after the relaxations and effectively becomes fourfold coordinated.

5. The (1 0 1) surface

We find that the low-energy cut for the (1 0 1) surface terminates at the point (0, 0, 0) with a calculated surface energy of 0.62 J/m^2. A slab of 9.7 Å with a relaxation layer of 2.6 Å is sufficient. Another cut terminates at point (0, 0, 0.5) but provides a much higher energy of 1.35 J/m^2. The relaxed structure of the low-energy termination is shown in Fig. 6 and the relaxations are given in Table II. The surface cuts through the Fe and Li octahedra, and leaves threefold $Li_{(1)}$ and $Li_{(2)}$ together with fivefold $Fe_{(1)}$ and fourfold $Fe_{(2)}$ on the surface. The dominating relaxations are the inward displacements of the threefold $Li_{(1)}$, $Li_{(2)}$, and the fourfold $Fe_{(2)}$. The fivefold $Fe_{(1)}$ undergoes minor relaxations compared to other undercoordinated atoms on the surface.

6. The (1 1 0) surface

There are two possible cutting options for the (1 1 0) surface: one terminates at point (0, 0, 0) and the other terminates at point (0.5, 0, 0). Note that there is mirror symmetry located at $(x,1/4,z)$, and n glide symmetry perpendicular to the a axis located at $(1/4,y,z)$. Points $(x,1-x,z)$ are therefore symmetrically equivalent to points $(x,x-1/2,z)$ through mirror symmetry, and further equivalent to points $(1/2-x,x,z+1/2)$ through the n glide symmetry. Hence, the two cuts actually provide the same surface structure. A slab of 10.5 Å with a relaxation layer of 3.2 Å is used. The relaxed structure of (1 1 0) surface is shown in Fig. 7 and the relaxations are given in Table II. The most significant relaxation is the displacement of fourfold $Li_{(1)}$ in the [1−1 0] direction. The distance between $Li_{(1)}$ and $Fe_{(1)}$ is increased from 3.309 to 5.068 Å after relaxation. This is again because of the strong electrostatic repulsion between $Li_{(1)}$ and $Fe_{(1)}$.

7. The (1 1 1) surface

There are two types of cuts for the (1 1 1) surface, one terminates at point (0, 0, 0) and the other terminates at point (0.5, 0, 0). While the former termination cuts right through the centers of PO_4 tetrahedra and creates a rather corrugated surface in order to preserve the PO_4 tetrahedra, the latter termination cuts right through centers of the LiO_6 and FeO_6 octahedra and creates a relatively flat surface. The surface energies are calculated to be 0.91 J/m^2 for the former termination and 0.85 J/m^2 for the latter one. The low-energy cut is shown in Fig. 8 and the relaxations are given in Table II. A slab of 11.5 Å with a relaxation layer of 3.2 Å is used. Most atoms on the surface undergo inward displacements except for the $P_{(1)}$ atom.

8. The (2 0 1) surface

We find that the low-energy cut for the (2 0 1) surface terminates at the point (0, 0, 0) [also across the symmetrically equivalent point (0.5, 0, 0)] with a calculated surface energy of 0.52 J/m^2. This is the lowest value of the surface energies we found. To obtain a converged number, a slab of 10.9 Å with a relaxation layer of 3.2 Å is used. Another

FIG. 8. (Color online) The relaxed surface structure of (1 1 1) surface.

TABLE V. Calculated redox potentials for the extraction of Li from five surfaces of $LiFePO_4$ as well as the bulk potential.

Orientation	(100)	(010)	(101)	(011)	(201)	bulk
Voltage (V)	3.84	**2.95**	3.25	3.79	3.76	3.55

this delithiation process on the surface can be calculated as

$$V = -\frac{G[(\mathrm{LiFePO_4})_n] - G[(\mathrm{Li})_{n-m}(\mathrm{FePO_4})_n]}{m} + \mu^{\circ}(\mathrm{Li}), \tag{4}$$

where G is the Gibbs free energy of the slab and $\mu^{\circ}(\mathrm{Li})$ is the anode reference chemical potential for Li. Typically, the Gibbs free energy can be replaced by the ground-state energy.[51] In this study, we calculate the Li redox potentials only for the five surfaces that appear in our Wulff shape. In practice, all the Li atoms on the top (and also symmetrically equivalent Li atoms on the bottom) outermost layer of each slab are extracted: that is, $Li_{(1)}$ and $Li_{(2)}$ (see Fig. 6) for the (1 0 1) surface, and $Li_{(1)}$ (see Figs. 2, 3, 5, and 9) for the other four surfaces. Therefore, the calculated surface redox potentials should be interpreted as the average redox potentials to extract/insert Li from/into the outermost layer of a given surface. The results (see Table V) show that the redox potentials for different surfaces range from 2.95 to 3.84 V, compared with the calculated Li insertion/deinsertion redox potential of 3.55 V in the bulk. Among these five surfaces, the (0 1 0) direction has the lowest potential, indicating the energetic preference of extracting Li from this surface.

IV. DISCUSSIONS

The surfaces we have investigated cut through LiO_6 and FeO_6 tetrahedra, leaving undercoordinated Li and Fe exposed on the surfaces. The energy of a surface can be lowered by increasing the bonding strength between the undercoordinated cations and nearby O atoms. Typically, this bond strengthening is observed as a shortened bond length after surface relaxation on most surfaces we studied. The undercoordinated Li atoms are most likely to undergo large in-plane displacements on the surface. The coordination of $Li_{(1)}$ (see Fig. 2) on the (1 0 0) surface is reduced from three to two, and the fivefold coordinated $Li_{(2)}$ (see Fig. 5) on the (0 1 1) surface becomes fourfold coordinated after the relaxation. An extra Li-O bond is formed on the (1 1 0) surface and increases the coordination of one Li ($Li_{(1)}$ in Fig. 7) from 3 to 4. In contrast, the undercoordinated Fe atoms usually lower their energies by inward displacements towards the bulk.

Our simple model developed to fit the surface energy in terms of coordination changes of Li and Fe shows that coordination loss is energetically more unfavorable for Fe atoms than it is for Li. Therefore, a low-energy surface generally has fewer Fe-O bonds affected by the surface cut. This statement is verified by comparing the coordination change per area for different surfaces. For example, the low-energy (0 1 0) surface has a Fe coordination number loss of about 4.0 bonds per nm^2, compared with a value of about 6.3 bonds per nm^2 for the high energy (0 0 1) surface. The surfaces that leave threefold coordinated Fe exposed [e.g., the (0 0 1) and (1 1 0) surfaces] are calculated to be high-energy surfaces. The coordination based energy expansion in Eq. (2) also allows us to deduce from the *ab initio* computations that the energy to create undercoordinated Fe on the surface approximately scales with its degree of undercoordination. The displacements for Fe on the surface are generally small, so that the energy of a surface cannot be effectively lowered by the local relaxations of the undercoordinated Fe atoms. Conversely, the undercoordinated Li can lower the energy of a surface by more freely relaxing. This is partially reflected in our fitting model where the undercoordinated Li atoms contribute quite differently from the Fe to the surface energies. Undercoordinated Li atoms on the surface are somehow beneficial to reduce the energy of the surface cut, and the fivefold Li is found to be the lowest-energy configuration on the surface. This may be a reflection of the general fact that the potential to extract Li from tetrahedral sites is higher than for octahedral sites in bulk materials, as can be observed by comparing Li voltages for spinels and layered oxides with the same active redox couple.[52] Therefore, it is not surprising to see that undercoordinated Li has a negative energy contribution to the surface energy in our model. All else being equal, sixfold is not the preferred coordination for Li. The importance of our fitting model for the surfaces of $LiFePO_4$ also lies in its ability to predict the energetics of high-index surfaces, which are computationally challenging in DFT. As a test, the surface energy in the high-index [4 0 1] orientation is calculated using both our fitting model and *ab initio* methods. For the unrelaxed (4 0 1) surface (with a base area of 131 A^2), there are two threefold Fe ions, one fourfold Fe ion, and two fivefold Fe ions, together with one threefold Li ion and two fivefold Li ions. Applying the fitted parameters given in Table III, we predict the surface energy in the [4 0 1] direction to be 1.29 J/m^2, which is in good agreement with the value of 1.15 J/m^2 calculated using the direct *ab initio* approach, even though the latter value was not used in the fit.

It is likely that the Wulff shape will vary somewhat with chemical environment. Our calculations are for stoichiometric surfaces at zero K. In particular, environments that cause partial oxidation of the surface could modify the Wulff shape of the crystal. A hint of this can be observed by comparing the surface energies of $FePO_4$ (Table IV) with those of $LiFePO_4$ (Table I). For $FePO_4$ the ratio of the (0 1 0) surface energy to the surface energy of any of the facets perpendicular to it [e.g., (2 0 1) surface] is much smaller than for $LiFePO_4$, indicating a more extreme aspect ratio for the Wulff shape of $FePO_4$ with a larger contribution of the (0 1 0) facet to total surface area. Note that oxidation (Li removal) does not occur at the same potential for all surfaces, creating the possibility that under some conditions several surfaces would be lithiated while others might be free of Li. In addition, given the importance of oxygen coordination of the exposed cations for the surface energy, the adsorption of O-containing species (e.g., OH^- and H_2O) is likely to affect the surface energy in aqueous environments such as hydrothermal synthesis.

Finally, we believe that our calculations of surface redox potentials can provide insights into the possible Li insertion/deinsertion mechanisms, particularly for materials with small particle size, where surface effects on the lithiation thermodynamics are expected to be significant. The Li redox potential for the (0 1 0) surface is 2.95 V, significantly lower than the calculated bulk value of 3.55 V. Spin density integrations for the delithiated (0 1 0) surface further confirm that the hole (Fe^{3+}) created when the threefold Li ($Li_{(1)}$ in Fig. 3) is extracted from the surface locates at the fivefold Fe ($Fe_{(2)}$ in Fig. 3). On the (0 1 0) surface the threefold Li shares edges with both the PO_4 tetrahedron and the capped FeO_6 octrahedron ($Fe_{(2)}$ in Fig. 3). The edge-sharing between the threefold Li and fivefold Fe further increases the energy of the threefold Li, and contributes to the decrease in the redox potential for the (0 1 0) surface. We performed similar redox potential calculations for the *insertion* of Li on the (0 1 0) surface of $FePO_4$ and found it to be 2.95 V. Hence, we expect that for a well-faceted $LiFePO_4$ particle, Li will be first extracted from the (0 1 0) surface upon charging and inserted last upon discharging. Furthermore, the same energetic considerations suggest that in the discharging process, any Li on the (0 1 0) surface would move deeper into the bulk where its potential (energy) is higher (lower). Such a mechanism may be beneficial for rapid discharge as the (0 1 0) direction is the only direction along which Li can propagate into the bulk.[2] Hence, any clearing of the surface upon charge and discharge should facilitate Li motion across the surface layer.

Interestingly, the redox potential is not below the bulk value for all surfaces. For three of the five surfaces in the Wulff shape, the stronger Li binding caused by the undercoordination does lead to a higher potential (Table V) than the bulk, and hence the intuitive idea that ions at surfaces are less strongly bound may have to be abandoned. These surfaces will be lithiated for most of the charge/discharge cycle and may therefore form an obstacle to rapid Li insertion/extraction from the particle.

Our results reveal the importance of controlling not only the size of $LiFePO_4$ but also the morphology. Given the highly anisotropic nature of this material, maximizing the exposure of some surfaces over others may be very beneficial for optimal rate capability.

ACKNOWLEDGMENTS

This work was supported by the Assistant Secretary for Energy Efficiency and Renewable Energy, Office of FreedomCAR and Vehicle Technologies of the U.S. DOE under Contract No. DE-AC03-76SF00098, via subcontracts No. 6517748 and No. 6517749 with the Lawrence Berkeley National Laboratory. We would like to acknowledge the support from the Center for Materials Science and Engineering, MIT, and the NSF MRSEC program of the NSF under Contract No. DMR 02-13282. Additional computation resources were provided by the National Partnership for Advanced Computing Infrastructure (NPACI). We also thank G. Chen and T. J. Richardson for providing valuable unpublished experimental information. At the time of the resubmission of this manuscript, we also became aware that surface calculations with empirical potentials by Islam *et al.* at the University of Bath, seem to also find low surface energies for the (0 1 0), (0 1 1), and (2 0 1) facets.[53]

*Author to whom correspondence should be addressed. gceder@mit.edu

[1] T. Maxisch and G. Ceder, Phys. Rev. B **73**, 174112 (2006).
[2] D. Morgan, A. Van der Ven, and G. Ceder, Electrochem. Solid-State Lett. **7**, A30 (2004).
[3] M. S. Islam, D. J. Driscoll, C. A. J. Fisher, and P. R. Slater, Chem. Mater. **17**, 5085 (2005).
[4] R. Amin, P. Balaya, and J. Maier, Electrochem. Solid-State Lett. **10**, A13 (2006).
[5] S. Y. Chung, J. T. Bloking, and Y. M. Chiang, Nat. Mater. **1**, 123 (2002).
[6] H. Huang, S. C. Yin, and L. F. Nazar, Electrochem. Solid-State Lett. **4**, A170 (2001).
[7] J. Barker, M. Y. Saidi, and J. L. Swoyer, Electrochem. Solid-State Lett. **6**, A53 (2003).
[8] P. S. Herle, B. Ellis, N. Coombs, and L. F. Nazar, Nat. Mater. **3**, 147 (2004).
[9] A. Yamada, S. C. Chung, and K. Hinokuma, J. Electrochem. Soc. **148**, A224 (2001).
[10] C. Delacourt, P. Poizot, S. Levasseur, and C. Masquelier, Electrochem. Solid-State Lett. **9**, A352 (2006).
[11] S. Yang, P. Y. Zavalij, and M. S. Whittingham, Electrochem. Commun. **3**, 505 (2001).
[12] J. Chen and M. S. Whittingham, Electrochem. Commun. **8**, 855 (2006).
[13] S. Franger, F. Le Cras, C. Bourbon, and H. Rouault, Electrochem. Solid-State Lett. **5**, A231 (2002).
[14] S. Tajimi, Y. Ikeda, K. Uematsu, K. Toda, and M. Sato, Solid State Ionics **175**, 287 (2004).
[15] G. Meligrana, C. Gerbaldi, A. Tuel, S. Bodoardo, and N. Penazzi, J. Power Sources **160**, 516 (2006).
[16] K. Dokko, S. Koizumi, K. Sharaishi, and K. Kanamura, J. Power Sources **165**, 656 (2007).
[17] K. Dokko, S. Koizumi, and K. Kanamura, Chem. Lett. **35**, 338 (2006).
[18] G. Chen, X. Song, and T. J. Richardson, Electrochem. Solid-State Lett. **9**, A295 (2006).
[19] M. Ramamoorthy, D. Vanderbilt, and R. D. King-Smith, Phys. Rev. B **49**, 16721 (1994).
[20] A. Christensen and E. A. Carter, Phys. Rev. B **58**, 8050 (1998).
[21] I. Batyrev, A. Alavi, and M. W. Finnis, Faraday Discuss. **114**, 33 (1999).
[22] X. G. Wang, A. Chaka, and M. Scheffler, Phys. Rev. Lett. **84**, 3650 (2000).
[23] A. Marmier and S. C. Parker, Phys. Rev. B **69**, 115409 (2004).
[24] G. Wulff, Z. Kristallogr. Mineral. **34**, 449 (1901).
[25] P. E. Blöchl, Phys. Rev. B **50**, 17953 (1994).
[26] G. Kresse and J. Furthmüller, Phys. Rev. B **54**, 11 169 (1996).

[27] F. Zhou, C. A. Marianetti, M. Cococcioni, D. Morgan, and G. Ceder, Phys. Rev. B **69**, 201101(R) (2004).
[28] F. Zhou, M. Cococcioni, C. A. Marianetti, D. Morgan, and G. Ceder, Phys. Rev. B **70**, 235121 (2004).
[29] T. Maxisch, F. Zhou, and G. Ceder, Phys. Rev. B **73**, 104301 (2006).
[30] L. Wang, T. Maxisch, and G. Ceder, Phys. Rev. B **73**, 195107 (2006).
[31] F. Zhou, T. Maxisch, and G. Ceder, Phys. Rev. Lett. **97**, 155704 (2006).
[32] V. I. Anisimov, J. Zaanen, and O. K. Andersen, Phys. Rev. B **44**, 943 (1991).
[33] V. I. Anisimov, F. Aryasetiawan, and A. I. Liechtenstein, J. Phys.: Condens. Matter **9**, 767 (1997).
[34] O. Bengone, M. Alouani, P. Blöchl, and J. Hugel, Phys. Rev. B **62**, 16392 (2000).
[35] M. Cococcioni and S. de Gironcoli, Phys. Rev. B **71**, 035105 (2005).
[36] A. G. Petukhov, I. I. Mazin, L. Chioncel, and A. I. Lichtenstein, Phys. Rev. B **67**, 153106 (2003).
[37] A. I. Liechtenstein, V. I. Anisimov, and J. Zaanen, Phys. Rev. B **52**, R5467 (1995).
[38] G. Rousse, J. Rodriguez-Carvajal, S. Patoux, and C. Masquelier, Chem. Mater. **15**, 4082 (2003).
[39] D. Dai, M. H. Whangbo, H. J. Koo, X. Rocquefelte, S. Jobic, and A. Villesuzanne, Inorg. Chem. **44**, 2407 (2005).
[40] P. W. Tasker, J. Phys. C **12**, 4977 (1979).
[41] D. C. Sayle, D. H. Gay, A. L. Rohl, C. R. A. Catlow, J. H. Harding, M. A. Perrin, and P. Nortier, J. Mater. Chem. **6**, 653 (1996).
[42] P. M. Oliver, G. W. Watson, E. T. Kelsey, and S. C. Parker, J. Mater. Chem. **7**, 563 (1997).
[43] E. Heifets, R. I. Eglitis, E. A. Kotomin, J. Maier, and G. Borstel, Surf. Sci. **513**, 211 (2002).
[44] S. Hamad, S. Cristol, and C. R. A. Callow, J. Phys. Chem. B **106**, 11002 (2002).
[45] A. Hung, J. Muscat, I. Yarovsky, and S. P. Russo, Surf. Sci. **520**, 111 (2002).
[46] A. Eichler and G. Kresse, Phys. Rev. B **69**, 045402 (2004).
[47] R. A. Evarestov, E. A. Kotomin, D. Fuks, J. Felsteiner, and J. Maier, Appl. Surf. Sci. **238**, 457 (2004).
[48] A. Soon, M. Todorova, B. Delley, and C. Stampfl, Phys. Rev. B **75**, 125420 (2007).
[49] A. B. Mukhopadhyay, J. F. Sanz, and C. B. Musgrave, Phys. Rev. B **73**, 115330 (2006).
[50] G. Strang, *Applied Mathematics and Scientific Computing* (Wellesley-Cambridge Press, Wellesley, MA, 2006).
[51] M. K. Aydinol, A. F. Kohan, and G. Ceder, J. Power Sources **68**, 664 (1997).
[52] S. K. Mishra and G. Ceder, Phys. Rev. B **59**, 6120 (1999).
[53] C. A. J. Fisher and M. S. Islam, 16th International Conference on Solid State Ionics, Abstract No. 55, Shanghai, China, 2007 (unpublished).